Direct Observation of Entropy Driven Electron-Hole Pair Separation at an Organic Semiconductor Interface

Nicholas R. Monahan, Kristopher W. Williams, Bharat Kumar, Colin Nuckolls, X.-Y. Zhu

Department of Chemistry, Columbia University, 3000 Broadway, NY 10027, USA

Abstract

How an electron-hole pair escapes the Coulomb potential at a donor/acceptor interface has been a key issue in organic photovoltaic research. Recent evidence suggests that long-distance charge separation can occur on ultrafast timescales, yet the underlying mechanism remains unclear. Here we use charge transfer excitons (CTEs) across an organic semiconductor/vacuum interface as a model and show that nascent hot CTEs can spontaneously climb up the Coulomb potential within 100 fs. This process is driven by entropic gain due to the rapid rise in density of states with increasing electron-hole separation. In contrast, the lowest CTE cannot delocalize, but undergoes self-trapping and recombination.

Charge generation in organic photovoltaic (OPV) devices is contingent upon the dissociation of excitons into charge-separated states across donor/acceptor (D/A) interfaces, a process that can occur on femtosecond timescales with near unity quantum efficiency [1-3]. However, such rapid formation of charge-separated states appears contrary to the excitonic nature of the materials that comprise organic solar cells [4]. Given their low dielectric constants, it is not immediately obvious how the electron-hole pair is able to escape the poorly screened Coulomb potential that can give rise to charge transfer excitons (CTEs) with binding energies an order of magnitude higher than thermal energy at room temperature [5-9]. Recent experimental [10-14] and theoretical [15-17] studies suggest that electronic delocalization enables the electron-hole pair to escape the CTE trap and promotes long-range charge separation, in agreement with the Onsager model for ionization in solution [18]. Excess energy from the offset in energy levels at the donor/acceptor interface [10-17] or from the initial excitation photon [19, 20] is believed to assist long-range charge separation. The electron-hole pair in the CTE trap can also dissociate with the help of an additional photoexcitation step [21]. Despite this progress, the exact mechanism of long-range electron-hole pair formation at donor/acceptor interfaces remains

poorly defined and there are also seemingly contradicting findings of photo-carrier generation from low energy CTEs that are supposedly trapped [22-24]. In the latter case, there is likely a potential energy gradient that counters the Coulomb potential [25-28]. One universally present driving force for photo-carrier generation, which may be partially responsible for the initial long-range charge separation or the subsequent escape from the CTE trap, may be the entropic gain with increasing electron-hole separation [1, 29]. However, there has been little experiment evidence for this proposal.

Here we provide the first direct time domain view of entropy-driven charge separation using the model system of CTEs at a molecular semiconductor/vacuum interface. In this system, a molecular semiconductor is the donor and the free-electron like image potential state (IPS) band is the acceptor [9]. The electron is bound by both its mutual Coulomb interaction with the residual hole in the highest occupied molecular orbital (HOMO) of the molecule and the induced polarization (i.e., image potential) of the molecular semiconductor film. The main difference between this model system and an organic D/A interface lies in the extent of delocalization: the electron acceptor in our model system is the highly delocalized (parallel to the surface) and free-electron like IPS band, while that at a true D/A interface is the lowest unoccupied molecular orbital (LUMO). Despite the necessity of delocalization in the LUMO band for efficient charge separation at D/A interfaces [10-17], the effective mass of an electron is the LUMO band is expected to be much heavier than that of a free electron. We emphasize that the CTE on an organic semiconductor surface is a qualitative model, not a quantitative mimic, for us to explore the physics of CTE at interfaces. Unlike the buried interface at a real organic donor/acceptor interface, the use of model CTEs on an organic semiconductor surface enables the experimental investigation by the powerful technique of time-resolved two-photon photoemission (TR-2PPE) spectroscopy, as demonstrated previously in our laboratory for crystalline pentacene and tetracene surfaces [30,31]. Using the solid thin film surface of the next in the acene series, hexacene [32], we carry out a quantitative analysis of electron energy as a function of pump-probe delay in the CTE manifold and show that an electron-hole pair optically excited below the delocalized IPS threshold can spontaneously climb up the Coulomb potential well on ultrafast time scales (~100 fs). This is in stark contrast to previous TR-2PPE studies of electron dynamics on surfaces that showed the decrease in electron energy with increasing time, attributed to electron energy relaxation on a heterogeneous landscape [33,34] or due to dynamic localization [35,36,37].

Charge-transfer excitons and image potential states at polarizable surfaces are well-described by the dielectric continuum approximation [9,30,31]. Accordingly, we eschew a molecular-level treatment of the hexacene film. Instead, it is represented as a homogeneous dielectric slab. The hole is treated as a point charge fixed in space within the hexacene layer and the electron is confined to the positive half-space (vacuum) by a potential at the dielectric slab/vacuum interface. The total interaction between the electron and hole is a sum of their screened Coulomb interaction (V_h) and the image potential (V_i) due to polarization of the surface [9]:

$$V_h(\rho, z) = -\frac{e^2}{4\pi\varepsilon_0} \frac{\gamma}{\sqrt{\rho^2 + (z-z_h)^2}}; \quad V_i(z) = -\frac{e^2\beta}{16\pi\varepsilon_0 z}, \tag{1}$$

where ρ is the in-plane radius and z_h (z) represents the distance between the hole (electron) and the interface in the surface-normal direction; $\gamma = 2/(\varepsilon + 1)$, $\beta = (\varepsilon - 1)/(\varepsilon + 1)$, and ε is the dielectric constant (5.84 for hexacene [38]). Since the effective mass of the hole in an organic semiconductor is expected to be much larger than that of a free electron, we approximate the reduced mass of the excitonic quasiparticle with the free electron mass and set the fixed hole position (z_h) so the binding energy of the lowest CTE matches the experimental value of -0.84
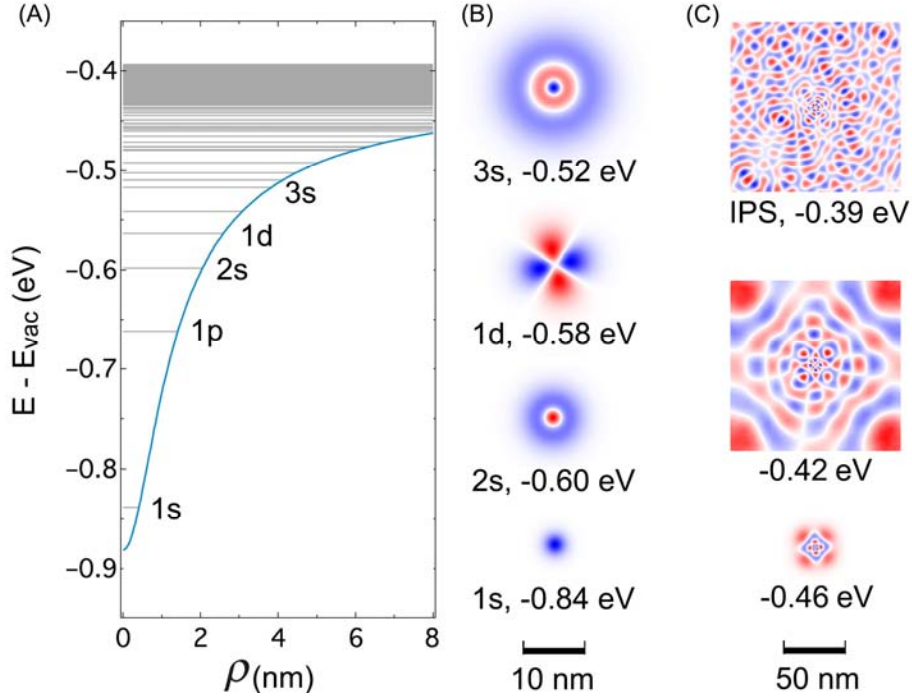

FIG. 1. (A) The effective potential $V_{i+h}(\rho)$ cut at z = 2.7 Å and associated eigenvalues. (B) xy-plane views of normalized eigenfunctions at z = 8 Å and corresponding binding energies for the first four dipole-allowed transitions (1s, 2s, 1d and 3s) from the hexacene HOMO. (C) xy-plane views of normalized eigenfunctions at z = 8 Å for the n = 1 IPS near $k_{\parallel} = 0$ (top), a highly-delocalized CTE (middle) and another CTE with a more moderate degree of delocalization (bottom). Note the different scale bars in (B) and (C).

eV (see below). We solve the Schrödinger equation using the finite element method in three dimensions (COMSOL MULTIPHYSICS, Comsol, Inc., Palo Alto). The resultant potential and eigenvalues are shown in Fig. 1A. The solutions represent a series of excitonic states that converge in energy towards a band of delocalized image potential states at 0.40 eV below the vacuum level, mimicking the nature of interfacial CTEs and charge-separated states at donor/acceptor interfaces in OPVs. Examples of the CTE and image potential state wave functions are shown in Fig. 1B and Fig. 1C. Although the first four dipole-allowed CTEs are localized in space, bound states closer to the bottom of the IPS band are highly delocalized and nearly occupy the entire 150 nm × 150 nm simulation cell. There is not a sharp transition

between excitonic and IPS states; the density of states (DOS) rises rapidly with increasing energy within the Coulomb potential.

The samples we use in the experiments are polycrystalline hexacene thin films vapor deposited on a bare Si(111) surface in ultrahigh vacuum (UHV). Each sample is transferred under UHV conditions to the analysis chamber that houses a hemispherical electron energy analyzer for 2PPE spectroscopy. The laser pulses come from a home built femtosecond non-collinear optical parametric amplifer (NOPA) pumped by a Yb-doped fiber laser (Clark-MXR Impulse). A more detailed description of the sample preparation and experimental setup is contained in the Supplemental Material [39]. One photon photoemission spectroscopy, Fig. 2A, shows the HOMO peak at -5.30 eV and the threshold (commonly referred to as conduction band maximum, or CBM) at approximately -5.0 eV (referenced to the vacuum level). For comparison, the CBM of pentacene thin film is at -5.15 eV [45], which is ~0.15 eV lower than that in hexacene, in agreement with band structure calculations [46]. A complete UP spectrum of hexacene is shown along with that of pentacene in Fig. S1 in the Supplemental Material [39].

In a TR-2PPE experiment, the first photon ($\hbar\omega_1 \geq 4$ eV) excites an electron from the HOMO of hexacene into the CTE-IPS manifold and the second photon ($\hbar\omega_2 = 1.48$ eV) ionizes these states. The 2PPE spectrum obtained at a pump-probe delay of 0 fs, Fig. 2B, reveals the CT_{1s} at -0.84 eV, the IPS (n=1) at -0.40 eV, and unresolved states in between. We track the dynamics of these states by varying the temporal delay between $\hbar\omega_1$ and $\hbar\omega_2$. Cross-correlations corresponding to
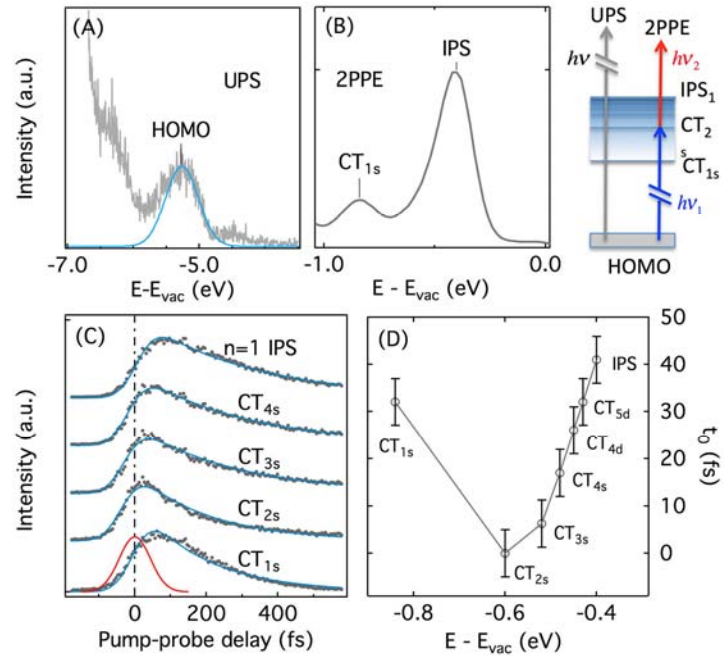
FIG 2. (A) Ultraviolet photoelectron spectrum (UPS, $\hbar\omega = 21.22$ eV) of hexacene on Si(111); the spectrum is shown in grey and a Gaussian fit to the HOMO is shown in blue. (B) 2PPE spectra at zero pump-probe delay for $\hbar\omega_1 = 4.70$ eV & $\hbar\omega_2 = 1.48$ eV showing the CT_{1s} and broad IPS/$CT_{\geq 2s}$ peaks. The schematic compares UPS with 2PPE spectroscopy. (C) Pump-probe cross-correlation traces from TR-2PPE ($\hbar\omega_1 = 4.70$ eV & $\hbar\omega_2 = 1.48$ eV) for CT_{1s}, CT_{2s}, CT_{3s} and CT_{4s} excitons as well as the n = 1 IPS fit to a convolution of a Gaussian pump-probe cross-correlation (100 fs FWHM, shown in red; t_0 is referenced to the zero delay from the CT_{2s} state) and an exponential decay. The dot-dashed line is $t_0 = 0$ fs. (D) The dependence of effective delay times on state energy.

energetic positions of several CTEs as well as the n=1 image potential state are compared in Fig. 2C. Fitting the experimental data to a convolution of a Gaussian pump-probe cross-correlation and a single exponential decay reveals that these states do not share a common zero time delay, t_0, i.e. they are not populated concurrently. Given the bandwidths of the excitation laser pulse ($\Delta E \sim 0.08$ eV) and the hexacene HOMO (~0.4 eV, see Gaussian fit in Fig. 2A), the pump photon energy of $\hbar\omega_1 = 4.7$ eV is resonant with CT_{2s}, but should also excite states within approximately ±0.2 eV of CT_{2s}. Although CT_{2s} (-0.60 eV) is formed promptly, the offset in peak position from time zero in Fig. 2C indicates that states with higher energy are sequentially populated. This is quantified in Fig. 2D, which shows the delay in formation time (t_0) as a function of state energy for a few selected CTE states and the IPS (n = 1). At the energetic extremes, the CT_{1s} and the n=1 IPS states are populated with time delays of 32±5 fs and 42±5 fs, respectively.

The temporal offset between CT_{2s} and CT_{1s} is readily explained by internal conversion within the CTE manifold, however the delayed formation (by 43 fs) of the IPS, located at ~0.2 eV above the center-of-gravity of the initial excitation, requires a more involved description. A similar observation was made earlier by Yang *et al.* for the pentacene monolayer grown on Bi(111), where the delayed formation of the IPS was interpreted as due to initial photo-excitation in the semimetal bismuth substrate followed by electron transfer to the IPS [31]. However, the use of a 10 nm thick hexacene film on the semiconducting Si(111) surface in the present case precludes this possibility. Instead, the delayed rise in IPS population must come from the CTE states. This
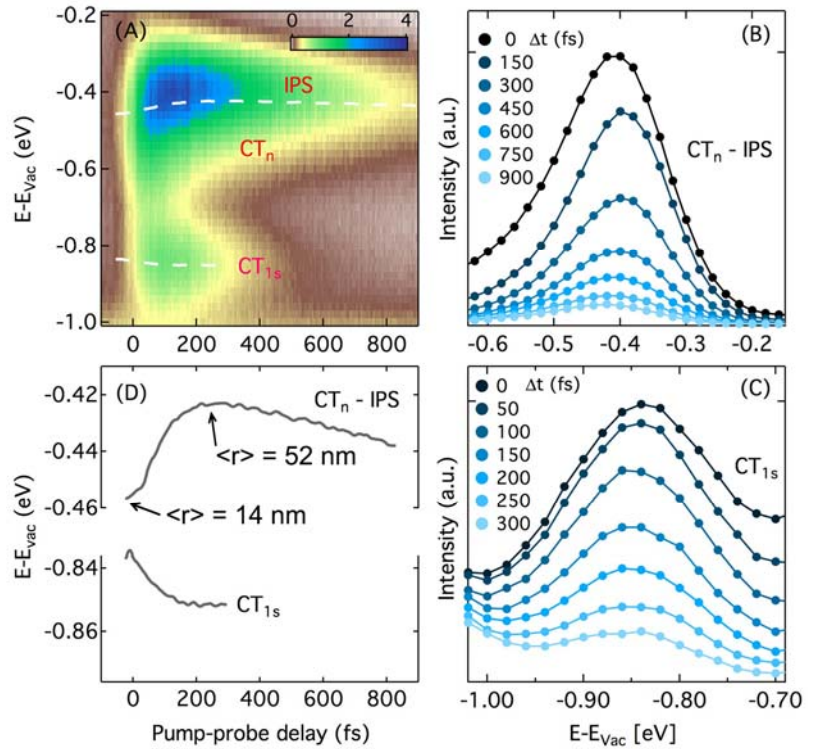
FIG. 3 **(a)** Two dimensional false-color plot of TR-2PPE spectra collected with for $\hbar\omega_1 = 4.70$ eV. (b) The evolution of the IPS/$CT_{\geq 2s}$ with pump-probe delay. After increasing in energy, the peak center monotonically decreases. (c) The evolution of the CT_{1s} peak with pump-probe delay. Unlike the higher energy states, the CT_{1s} exciton only decreases in energy. (d) Comparison of IPS/$CT_{\geq 2s}$ (top) and CT_{1s} (bottom) peak centers of mass as a function of pump-probe delay time. The IPS/$CT_{\geq 2s}$ peak center shifts up in energy 30 meV from time-delay zero (τ =73±5 fs), after which it relaxes by 16±5 meV. The CT_{1s} state relaxes 15±5 meV within approximately 100 fs.

means that excited electrons above the hexacene surface must ascend the Coulomb potential on a short time scale.

We now analyze the rise in energy of the electron. Fig. 3A shows a 2D pseudo-color plot of TR-2PPE spectra as functions of state energy and pump-probe delay. The broad spectral feature between CT_{2s} and IPS shows an upward shift in peak position (blue) within ~200 fs, in contrast to the downward movement of the CT_{1s} peak. Although the excitation photon energy is resonant with the CT_{2s} exciton at -0.60 eV, there is clearly spectral intensity from more energetic CT_n states that extends to the IPS. Note the intensity from unresolved CT_n (n >2s) states is higher than that from the resonant CT_{2s}; this can be attributed to both the high DOS above CT_{2s} and indirect population from CT_{2s}. Spectra comprising this peak at a range of pump-probe delay times are shown in Fig. 3B. From this plot it is clear that the peak center shifts by an appreciable amount, first increasing in energy and then decreasing. A similar plot for the CT_{1s} exciton is shown in Fig. 3C, where the peak center undergoes only a monotonic decrease in energy as the pump-probe delay time increases.

We quantify the energetic evolution of the peak by its barycentric mean, as is common in fluorescence and vibrational spectroscopies. The temporal evolutions in the center-of-mass of the two peaks are shown as white dashed lines in Fig. 3A, and magnified in Fig. 3D. The CT_{1s} peak undergoes a 16±5 meV relaxation within ~100 fs of t_0. Though not large, this energy relaxation is consistent with the lattice relaxation energy of acenes [47, 48, 49] and can be attributed to localization of the hole by hole-polaron formation in the hexacene lattice. The result is a self-trapped CT_{1s} exciton, similar to exciton self-trapping in polarizable media [50]. In contrast to the behavior of CT_{1s}, the broad CT_{2s}-IPS peak initially increases in energy with a time constant of ~73±5 fs to a maximum of 33±5 meV above its position at t_0, followed by a slow decay of 15±5 meV in 600 fs. The latter can again be attributed to hole localization and the formation of a self-trapped CT exciton.

The increase in mean CT exciton energy on an ultrafast time scale (≤100 fs) indicates that the initially excited electron-hole pair must scale the Coulomb potential and become more delocalized. The laws of thermodynamics dictate that a spontaneous process must correspond to a decrease in free energy (Gibbs energy at constant pressure or Helmholtz energy at constant volume). In the present case, the increase in electron energy (or enthalpy) must be over-compensated by an increase in entropy. This condition is satisfied, as the DOS within the Coulomb potential increases rapidly with energy (Fig. 1), leading to the spontaneous separation of the electron-hole pair. Further supporting this interpretation, we find that the CT_{1s} exciton does not undergo such a spontaneous delocalization process, because it is energetically isolated in the Coulomb potential. There are no other states within ~0.24 eV from the CT_{1s} state and the CT_{1s} undergoes recombination with a time constant of ~100 fs, as determined by intensity decay. For completeness, we point out that the electronic degrees of freedom depicted in Fig. 1 are in constant interaction with the phonon bath. The absorption of low-energy lattice phonons is responsible for the initial rise in electronic energy and the corresponding electron-hole

separation, while the emission of phonons is responsible for the subsequent relaxation and self-trapping of the CT exciton. For the linear acenes, the low energy modes correspond to molecular translation and libration with energies ranging from ~3 meV up to ~20 meV, while the high energy modes correspond to intra-molecular bond stretching with energies in the a few hundred meV range [51,52]. Interestingly, we find that the rise in the broad CT_{2s}-IPS peak is insensitive to temperature in the 120-298 K range (Fig. S3 in Supplemental Material [39]). We believe the phonon modes responsible for the initial CTE delocalization are likely populated by the dissipation of excess intramolecular vibrational energy created during photoexcitation [53, 54]. In essence, photoexcitation creates a local lattice temperature that is higher than that of the bulk. This surplus of lattice modes leads to temperature-independent delocalization dynamics.

To estimate the extent of spontaneous delocalization and electron-hole separation, we calculate the mean radius, <r>, using the eigenfunctions from Fig. 1. The mean radii are 6.4 nm for the resonant CT_{2s} state and 14 nm for states near the center-of-mass (-0.46 eV) t = 0 fs. The <r> increases to 52 nm for states near the center-of-mass (-0.42 eV) at t = 100 fs. Consequently, the delocalization corresponds to a nearly fourfold increases in the average electron-hole separation (*mostly in the surface plane*) within 100 fs, a spontaneous process driven by the entropic increase as the electron-hole pair rises in the Coulomb potential. Although the ultrafast separation of an electron-hole pair has been suggested as key to efficient charge separation at donor/acceptor interfaces in OPVs [10-17], our finding provides the first direct view of such a delocalization process in the time-domain. The entropic driving force should be universal to charge separation at donor/acceptor interfaces.

References

1   T. M. Clarke and J. R. Durrant, Chem. Rev. **110**, 6736 (2010).

2   J. L. Brédas, J. E. Norton, J. Cornil, and V. Coropceanu, Acct. Chem. Res. **42**, 1691 (2009).

3   N. Banerji, J. Mater. Chem. C **1**, 3052 (2013).

4   V. I. Arkhipov and H. Bässler, Phys. Status Solidi A **201**, 1152 (2004).

5   A. C. Morteani, P. Sreearunothai, L. M. Hertz, R. H. Friend, and C. Silva, Phys. Rev. Lett. **92**, 247402 (2004).

6   K. Tvingstedt, K. Vandewal, A. Gadisa, F. Zhang, J. Manca, and O. Inganas, J. Am. Chem. Soc. **131**, 11819 (2009).

7   M. A. Loi, S. Toffanin, M. Muccini, M. Forster, U. Scherf, and M. Scharber, Adv. Funct. Mater. **17**, 2111 (2007).

8   T. Drori, C.-X. Sheng, A. Ndobe, S. Sinh, J. Holt, and Z. V. Vardeny, Phys. Rev. Lett. **101**, 03740 (2008).

9   X.-Y.; Zhu, Q. Yang, and M. Muntwiler, Acct. Chem. Res. **42**, 1779 (2009).

10   A. Jailaubekov, A. P. Willard, J. Tritsch, W.-L. Chan, N. Sai, R. I. Gearba, L. G. Kaake, K. J. Williams, K. Leung, P. J. Rossky, and X.-Y. Zhu, Nat. Mater. **12**, 66 (2013).

11   S. Gélinas, A. Rao, A. Kumar, S. L. Smith, A. W. Chin, J. Clark, T. S. van der Poll, G. C. Bazan, and R. H. Friend, Science **343**, 512 (2014).

12   S. M. Falke, C. A. Rozzi, D. Brida, M. Maiuri, M. Amato, E. Sommer, A. De Sio, A. Rubio, G. Cerullo, E. Molinari, and C. Lienau, Science **344**, 1001 (2014).

13   F. Provencher, N. Bérubé, A. W. Parker, G. M. Greetham, M. Towrie, C. Hellmann, M. Côté, N. Stingelin, C. Silva, and S. C. Hayes, Nat. Commun. **5**, 4288 (2014).

14   B. Bernardo, D. Cheyns, B. Verreet, R. D. Schaller, B. P. Rand, and N. C. Giebink, Nat. Commun. **5**, 3245 (2014).

15   H. Tamura and I. Burghardt, J. Am. Chem. Soc. **135**, 16364 (2013).

16   E. R. Bittner and C. Silva, Nat. Commun. **5**, 3119 (2014).

17   B. M. Savoie, A. Rao, A. A. Bakulin, S. Gelinas, B. Movaghar, R. H. Friend, T. J. Marks, and M. A. Ratner, J. Am. Chem. Soc. **136**, 2876 (2014).

18   L. Onsager, Phys. Rev. **54**, 554 (1938).

19   G. Grancini, M. Maiuri, D. Fazzi, A. Petrozza, H.-J. Egelhaaf, D. Brida, G. Cerullo, and G. Lanzani, Nat. Mater. **12**, 29 (2013).

20   T. Hahn, J. Geiger, X. Blase, I. Duchemin, D. Niedzialek, S. Tscheuschner, D. Beljonne, H. Bässler, A. Köhler. Advanced Functional Materials 25, 1287 (2015).

21   A. A. Bakulin, A. Rao, V. G. Pavelyev, P. H. M. van Loosdrecht, M. S. Pshenichnikov, D. Niedzialek, J. Cornil, D. Beljonne, and R. H. Friend, Science **335**, 1340 (2012).

22   P. Parkinson, J. Lloyd-Hughes, M. Johnston, and L. Herz, Phys. Rev. B **78**, 115321 (2008).

23   J. Lee, K. Vandewal, S. R. Yost, M. E. Bahlke, L. Goris, M. A. Baldo, J. V Manca, and T. Van Voorhis, J. Am. Chem. Soc. **132**, 11878 (2010).

24   K. Vandewal, S. Albrecht, E. T. Hoke, K. R. Graham, J. Widmer, J. D. Douglas, M. Schubert, W. R. Mateker, J. T. Bloking, G. F. Burkhard, A. Sellinger, J. M. J. Fréchet, A. Amassian, M. K. Riede, M. D. McGehee, D. Neher, and A. Salleo, Nat. Mater. **13**, 63 (2014).

25   D. P. McMahon, D. L. Cheung, and A. Troisi, J. Phys. Chem. Lett. **2**, 2737 (2011).

26   S. R. Yost, L.-P. Wang, and T. Van Voorhis, J. Phys. Chem. C **115**, 14431 (2011).

27   W. Chen, T. Xu, F. He, W. Wang, C. Wang, J. Strzalka, Y. Liu, J. Wen, D. J. Miller, J. Chen, K. Hong, L. Yu, and S. B. Darline, Nano Lett. **11**, 3707 (2011).

28   T. M. Burke and M. D. McGehee. Adv. Mater. **26**, 1923 (2013).

29 B. A. Gregg, J. Phys. Chem. Lett. **2**, 3013 (2011).

30 M. Muntwiler, Q. Yang, W. Tisdale, and X.-Y. Zhu, Phys. Rev. Lett. **101**, 196403 (2008).

31 Q. Yang, M. Muntwiler, and X.-Y. Zhu, Phys. Rev. B **80**, 115214 (2009).

32 M. Watanabe, Y. J. Chang, S.-W. Liu, T.-H. Chao, K. Goto, M. M. Islam, C.-H. Yuan, Y.-T. Tao, T. Shinmyozu, and T. J. Chow, *Nature Chem.* **4**, 574 (2012).

33 U. Bovensiepen, C. Gahl, J. Stähler, M. Bockstedte, F. Baletto, A. Rubio, X.-Y. Zhu, S. Scandolo, and M. Wolf, *J. Phys. Chem. C* **113**, 979 (2009).

34 D. E. Suich, B. W. Caplins, A. J. Shearer, C. B. Harris. *J. Phys. Chem. Lett.*, **5**, 3073, (2014).

35 N. H. Ge, C. M. Wong, R. L. Lingle, J. D. McNeill, K. J. Gaffney, and C. B. Harris, *Science* **279**, 202-205 (1998).

36 A. D. Miller, I. Bezel, K. J. Gaffney, S. Garrett-Roe, S. H. Liu, P. Szymanski, and C. B. Harris, *Science* **297**, 1163-1166, (2002).

37 M. Muntwiler, and X.-Y. Zhu, *Phys. Rev. Lett.* **98**, 246801 (2007).

38 G. D'Avino, L. Muccioli, C. Zannoni, D. Beljonne, and Z. G. Soos, J. Chem. Theory Comput. **10**, 4959 (2014).

39 See Supplemental Material at [URL] for hexacene thin film preparation and characterization procedures in addition to a description of the ultrafast laser setup, which includes Refs. [40-44].

40 E. Busby, T. C. Berkelbach, B. Kumar, A. Chernikov, Y. Zhong, H. Hlaing, X.-Y. Zhu, T. F. Heinz, M. S. Hybertsen, M. Y. Sfeir, D. R. Reichman, C. Nuckolls, and O. Yaffe, J. Am. Chem. Soc. **136**, 10654 (2014).

41 F. J. Meyer zu Heringdorf, M. C. Reuter, and R. M. Tromp, Nature **412**, 517 (2001).

42 P. G. Schroeder, C. B. France, J. B. Park, and B. A. Parkinson, J. Phys. Chem. B **107**, 2253 (2003).

43 C. Homann, C. Schriever, P. Baum, and E. Riedle, Opt. Express **16**, 5746 (2008)

44 X.-Y. Zhu, Q. Yang, and M. Muntwiler, Acc. Chem. Res. **42**, 1779 (2009).

45 H. Kakuta, T. Hirahara, I. Matsuda, T. Nagao, S. Hasegawa, N. Ueno, and K. Sakamoto. Phys. Rev. Lett. **98**, 247601 (2007).

46 E. S. Kadantsev, M. J. Stott, and A. Rubio, *J. Chem. Phys.* **124**, 134901 (2006).

47 V. Coropceanu, M. Malagoli, D. A. da Silva Filho, N. E. Gruhn, T. G. Bill, and J. L. Brédas, Phys. Rev. Lett. 89, 275503 (2002).

48 J. Singh, *Excitation Energy Transfer Processes in Condensed Matter* (Plenum Press, New York, 1994), p. 146.

49   R. S. Sánchez-Carrera, P. Paramonov, G. M. Day , V. Coropceanu, and Jean-Luc Brédas, *J. Am. Chem. Soc.* **132**, 14437, (2010).

50   K. S. Song and R. T. Williams, *Self-Trapped Excitons*; Springer Series in Solid-State Sciences (Springer: Berlin, 1993), Vol. 105.

51   R. S. Sánchez-Carrera, P. Paramonov, G. M. Day , V. Coropceanu, and Jean-Luc Brédas, *J. Am. Chem. Soc.* **132**, 14437, (2010).

52   R. Guido Della Valle , E. Venuti , L. Farina , and A. Brillante, *J. Phys. Chem. B* **108**, 1822, (2004).

53   V. May and O Kühn, Charge and Energy Transfer Dynamics in Molecular Systems (WILEY-VCH, Weinhein, 2011), Sec. 5.3.

54   A. Nitzan, *Chemical Dynamics in Condensed Phases* (Oxford University Press, New York, 2006), Sec. 13.6.